Thermodynamic functions and pressure-temperature phase diagram of lithium alanates by *ab initio* calculations

Xuezhi Ke[1,2,*] and Changfeng Chen[1,†]
[1]*Department of Physics, University of Nevada, Las Vegas, Nevada 89154, USA*
[2]*Department of Physics, East China Normal University, Shanghai 200062, China*
(Received 23 February 2007; published 20 July 2007)

We report on a study of thermodynamic functions and phase stability of lithium alanates $LiAlH_4$ and Li_3AlH_6 using *ab initio* density-functional and quasiharmonic phonon calculations. The calculated thermodynamic functions are in good agreement with available experimental data and are used to study the decomposition reactions of these materials. The results show that the decomposition of $LiAlH_4$ is irreversible under all temperature and pressure conditions considered, indicating that a direct synthesis of $LiAlH_4$ from the solid reaction of $(\frac{1}{3}Li_3AlH_6+\frac{2}{3}Al+H_2)$ is not possible. Meanwhile, the calculated results suggest that Li_3AlH_6 can be used as a rechargeable hydrogen-storage medium under certain temperature and pressure conditions. We construct the temperature-pressure phase diagram and present a discussion in conjunction with an analysis of recent experimental results.

DOI: 10.1103/PhysRevB.76.024112 PACS number(s): 64.60.−i, 65.40.−b, 63.20.−e, 71.15.Mb

I. INTRODUCTION

The search for hydrogen-based fuel cells is a very active field of research in recent years.[1–18] For on-board mobile applications, the development of compact, light, and affordable containment is the key. Since the catalyzed $NaAlH_4$ was found to release hydrogen under moderate conditions,[2] complex hydrides based on Al and B have received considerable attention as possible hydrogen-storage media for mobile applications. One of the potential candidates is $LiAlH_4$, which releases hydrogen in two steps,

$$LiAlH_4 \overset{5.3\ \text{wt.}\ \%}{\Rightarrow} \frac{1}{3}Li_3AlH_6 + \frac{2}{3}Al + H_2, \quad (1)$$

$$Li_3AlH_6 \overset{2.6\ \text{wt.}\ \%}{\Rightarrow} 3LiH + Al + \frac{3}{2}H_2, \quad (2)$$

where the first reaction releases 5.3 wt % hydrogen and the second reaction releases 2.6 wt % hydrogen relative to $LiAlH_4$. Thus, this material has a total theoretical capacity of 7.9 wt % hydrogen. Taken alone, the second reaction of the decomposition of Li_3AlH_6 can produce 5.6 wt % hydrogen. All of these seem promising. There have been several experimental studies on the thermodynamic phase stability of these hydrides.[15–18]

On the theoretical side, there have been studies on the thermodynamic stability of these hydrides at atmospheric pressure. Based on the harmonic phonon approximation (HA) and first-principles calculations, Løvvik *et al.*[11] found that the calculated reaction enthalpy for Eq. (1) is positive, suggesting that this reaction is endothermic. Using the same approaches, Frankcombe and Kroes[12] found that the decomposition of $LiAlH_4$ is spontaneous even at low temperatures, and the hydrides $LiAlD_4$ and Li_3AlD_6 are more stable than those of $LiAlH_4$ and Li_3AlH_6, respectively. Recently, Jang *et al.*[14] used an empirical thermodynamic method to study the phase equilibrium between $LiAlH_4$ and Li_3AlH_6. It is noted that their empirical method is highly dependent on the existing thermodynamic data of these hydrides as input. However, such data for Li_3AlH_6 from experiment or accurate theoretical calculations are still lacking.

In this paper, we present first-principles calculations of the thermodynamic functions of these lithium alanates. The obtained results are in good agreement with available experimental data. These results are then used to study the phase stability and reaction reversibility relevant to practical operating conditions in their potential on-board mobile applications as hydrogen-storage media. The calculated data also provide the needed input for other (e.g., empirical) theoretical studies where experimental data are not yet available. In the present work, we are especially interested in the thermodynamic phase stability of the lithium alanates under different temperature and pressure conditions. In particular, concerning the phase stability for Eq. (2), the physical picture is still unclear based on available experimental results. In the experiment of Chen *et al.*,[15] this reaction was reported to be reversible and the reaction enthalpy of 0.43 eV per H_2 was measured. However, their results have not been reproduced by other groups. Very recently, using similar catalysts, Brinks *et al.*[16] reported that the equilibrium pressure for this reaction was at least 85 bars at 353 K. Therefore, the stability of these hydrides at different pressures and temperatures remains an unresolved issue. A clarification of this issue based on first-principles calculations is the main objective of the present work.

The remainder of this paper is organized in three subsections. In Sec. II, the theoretical methods are introduced. In Sec. III, the results are presented and discussed. We show the calculated thermodynamic functions and then use them to study the phase stability in Eqs. (1) and (2) at different pressures and temperatures. In Sec. IV, the concluding remarks are made.

II. THEORETICAL METHODS

The first-principles calculations have been performed in the framework of the density-functional theory[19,20] using the

generalized gradient approximation[21] (GGA) as implemented in the VASP code.[22,23] The interaction between the ion and electron is described by the all-electron projector augmented wave method.[24,25] The configurations Al $3s^2 3p^1$, Li $2s^1$, and H $1s^1$ are treated as the valence electrons. Brillouin-zone integrations were performed on the grid of Monkhost-Pack procedure.[26] For each supercell, a dense k-point mesh (the spacing of k points $<0.2/\text{Å}$) and a high plane-wave cutoff energy of 600 eV were used. For medium-size cells ($\sim 4.8 \times \sim 7.8 \times \sim 7.8$ Å^3 for $LiAlH_4$ and $\sim 5.6 \times \sim 5.6 \times \sim 5.6$ Å^3 for Li_3AlH_6), $6\times4\times4$ and $6\times6\times6$ k-point meshes were used for $LiAlH_4$ and Li_3AlH_6, respectively. A total-energy convergence of within 0.2 meV/f.u. was achieved (when compared with the results using the meshes of $8\times6\times6$ and $8\times8\times8$ for $LiAlH_4$ and Li_3AlH_6, respectively). For a larger supercell for phonon calculations ($\sim 10 \times \sim 10 \times \sim 10$ Å^3), a $2\times2\times2$ k-point mesh was used. In this case, a total-energy convergence within 0.1 meV/f.u. was achieved (when compared with the results using a $4\times4\times4$ k-point mesh). To calculate the phonons of $LiAlH_4$, a big supercell ($9.660\times15.590\times15.559$ Å^3) was found to be necessary. A smaller supercell ($9.660\times7.795\times7.780$ Å^3) was found to produce a negative frequency at the C and Z points of the first Brillouin zone (this problem could not be solved by treating Li $1s^2$ semicore state as valence).

To calculate the phonon density of states (DOS), we use a direct *ab initio* force-constant approach, which was implemented by Parlinski.[27,28] In this method a specific atom is displaced to induce the forces to act on the surrounding atoms, which are calculated via the Hellmann-Feynman theorem. The magnitude of the displacement of 0.03 Å was used in our calculations. Usually, the criterion is to use displacement which gives the largest Hellmann-Feynman forces on the order of ±0.5–0.8 eV/Å. For these lattices, the forces caused by the 0.03 Å displacement were found to be smaller than 0.8 eV/Å. The forces were collected to form the force-constant matrices and then dynamical matrices. Harmonic phonons were obtained from the diagonalization of the dynamical matrices. The internal energy ($E_{(T)}$) was evaluated from the integral of phonon DOS as follows:

$$E_{(T)} = \frac{1}{2} r \int_0^\infty \hbar\omega g(\omega) \coth\left(\frac{\hbar\omega}{2k_B T}\right) d\omega, \tag{3}$$

where $g(\omega)$ is the phonon DOS, r is the number of degrees of freedom in the unit cell, $\hbar$ is the Planck constant, k_B is the Boltzmann constant, and T is the temperature. Similar integrals can be applied to calculate the entropy and free energy.[29]

To construct the phase diagram, one needs to examine the Gibbs free energies of the alanates at different pressures and temperatures. To obtain these energies, we used the quasiharmonic approximation (QHA), i.e., the phonons are harmonic, but they are volume dependent (e.g., see Refs. 29–31). In our calculations, the lattice volume is expanded or compressed. In detail, for $LiAlH_4$, the volumes of 40.0, 50.0, 57.5, 62.5, 65.0, 68.0, 69.3, 70.5, 71.8, 75.5, and 83.8 Å^3/f.u. are considered. For Li_3AlH_6, the volumes of 60.0, 65.0, 75.0, 80.0, 82.5, 87.7, 90.0, 92.5, 95.0, 97.5, and 102.5 Å^3/f.u. are considered. For LiH, the volumes of 10.0, 13.0, 14.0, 15.0, 16.1, 16.5, 17.0, 18.0, 19.0, and 20.0 Å^3/f.u. are considered. For a given volume, the lattice parameters and the atomic coordinates are fully optimized until the forces are smaller than 0.0002 eV/Å. For each optimized structure, its thermodynamic functions as a function of temperature including the vibrational entropy ($S_{(T,V)}$), the internal energy ($E_{(T,V)}$), the enthalpy ($H_{(T,V)}$), and the Helmholtz free energy ($F_{(T,V)}$) are computed. These functions have the following relationships:

$$H_{(T,V)} = E_{(elec,V)} + E_{(T,V)} + pV, \tag{4}$$

$$F_{(T,V)} = E_{(elec,V)} + E_{(T,V)} - TS_{(T,V)}, \tag{5}$$

$$G_{(T,V)} = H_{(T,V)} - TS_{(T,V)}, \tag{6}$$

where $E_{(elec,V)}$ is the electronic energy of the unit cell at a given volume V obtained from the first-principles total-energy calculations, T is the temperature, p is the pressure, and $G_{(T,V)}$ is the Gibbs free energy at a given T and V. At zero pressure, the equilibrium volume and its thermodynamic functions at a given temperature T are obtained by minimizing the Helmholtz free energy $F_{(T,V)}$ with respect to volumes V. It is noted that for solids, the energy and volume differences between zero and atmospheric pressure are negligible, e.g., for $LiAlH_4$, the difference of volume is 0.001 Å^3/f.u. and the difference of energy is 0.1 meV/f.u. At elevated pressures, the pressure p at a given temperature T is evaluated from the Helmholtz free energy $F_{(T,V)}$,

$$p = \left(\frac{\partial F_{(T,V)}}{\partial V}\right)_{(T)}. \tag{7}$$

To study the reactions in Eqs. (1) and (2), one needs to know the Gibbs free energy of H_2 gas. At atmospheric pressure, the Gibbs free energy is calculated by

$$G_{(p_0=1\ \text{atm},T)}(H_2) = E_{elec}(H_2) + E_{zp}(H_2) + \Delta H_{(T)}(H_2) - T\Delta S_{(T)} \times (H_2), \tag{8}$$

where $E_{elec}(H_2)$ is the electronic energy of a H_2 molecule obtained from the total-energy calculations, $E_{zp}(H_2)$ is the zero-point energy of a H_2 molecule obtained from the phonon calculations, and $\Delta H_{(T)}(H_2)$ and $\Delta S_{(T)}(H_2)$ are the temperature-dependent enthalpy and entropy, respectively. The values of $\Delta H_{(T)}(H_2)$ and $\Delta S_{(T)}(H_2)$ can be obtained from the tabulated thermochemical data.[32] At elevated pressures, the calculations of the Gibbs free energy will be discussed in the later section.

Since these hydrides contain very light elements such as H and Li, the zero-point energy will be relatively large, which can expand the lattice constants. The calculated lattice parameters for the hydrides obtained with and without the inclusion of the zero-point energy (ZPE) are compiled in Table I. Overall, our calculated parameters are in good agreement with other calculations and experimental data. It can be seen from Table I that the lattice constants are slightly expanded due to the zero-point motions. To examine how much the ZPE expands the volume, the correlation between the

TABLE I. Comparison between the calculated and experimental lattice parameters for LiH ($Fm\bar{3}m$), $LiAlH_4$ ($P2_1/c$), and Li_3AlH_6 ($R\bar{3}$). The zero-point energy (ZPE) for LiH, $LiAlH_4$, and Li_3AlH_6 are 0.223, 0.833, and 1.333 eV/f.u., respectively. All units are in Å.

Parameters	0 K GGA		0 K GGA including ZPE		Expt.
			LiH		
	Current	Others[a]	Current	Others[a]	At 83 K[b]
a	4.011	3.998 (4.018)	4.098	4.090 (4.14±0.02)	4.067
			$LiAlH_4$		$LiAlD_4$
	Current	Others[c]	Current	Others	At 9 K[d]
a	4.830	4.837 (4.854)	4.923	Unavailable	4.817
b	7.795	7.809 (7.826)	7.917	Unavailable	7.802
c	7.780	7.825 (7.842)	7.851	Unavailable	7.821
β	111.778	112.137(111.878)	111.581	Unavailable	112.228
			Li_3AlH_6		Li_3AlD_6
	Current	Others[e]	Current	Others	At 9 K[f]
a	8.013	8.027(8.049)	8.155	Unavailable	8.071
c	9.458	9.467(9.453)	9.648	Unavailable	9.513

[a]In Refs. 33 and 13. Without considering the ZPE, 4.01 and 3.987 Å were obtained in Ref. 35 (GGA) and Ref. 34 (PBE), respectively. With the ZPE, 4.112 Å was obtained in Ref. 36 (PBE). In Ref. 37 (LDA), 3.879 Å and 3.958 Å were obtained with and without the inclusion of ZPE, respectively.
[b]In Ref. 38.
[c]In Refs. 11 and 39.
[d]In Ref. 40.
[e]In Refs. 12 and 41.
[f]In Ref. 42.

ZPE and the expanded volume ΔV for these hydrides at $T=0$ K is plotted in Fig. 1. The expanded volume ΔV is defined as the difference between the volume obtained with and without the inclusion of the ZPE. The expanded volume increases with the ZPE following a nearly linear relationship.

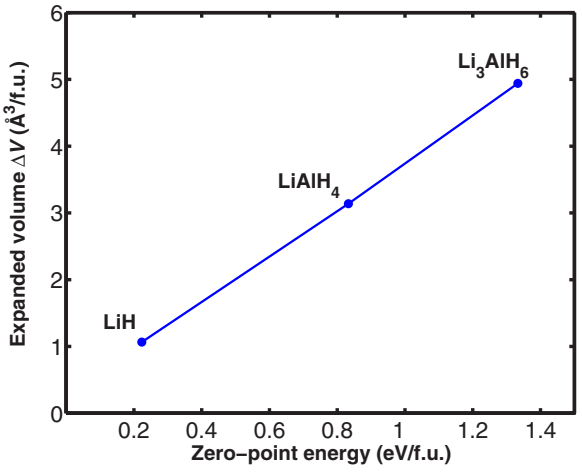

FIG. 1. (Color online) Correlation between the zero-point energy (ZPE) and its expanded volume ΔV for LiH, $LiAlH_4$, and Li_3AlH_6 at $T=0$ K. The expanded volume ΔV is defined as a volume difference between the volume obtained with and without the inclusion of the ZPE.

For Li_3AlH_6, its expanded volume ΔV is equal to 4.9 Å^3/f.u., which increases the free energy by 0.022 eV/f.u. at $T=0$ K. This effect will become more pronounced as temperature increases. Since a perfect harmonic crystal should not have any volume expansion under increasing temperature, this is apparently an anharmonic effect.[43] To some extent, this anharmonic effect can be taken into account by the QHA. Therefore, in principle, the results computed by the QHA are more accurate than those by the HA. Interestingly, a recent paper on $LiBH_4$ by Frankcombe and Kroes[13] reported that there is no significant difference between the results obtained from the QHA and from the HA at atmospheric pressure. We found a similar situation in our calculated results even at high temperatures. The reason for this phenomenon will be discussed below.

III. RESULTS AND DISCUSSION

A. Thermodynamic functions

We have calculated the volume-temperature curves for $LiAlH_4$, Li_3AlH_6, and LiH over a large range of temperature between 0 and 800 K. The results are shown in Fig. 2. By fitting these free-energy curves to the third order Birch-Murnaghan equation of state,[44] we can obtain the temperature-dependent equilibrium volume and thermal expansivity $\left(\alpha=\frac{1}{V}\frac{\partial V}{\partial T}\right)$, which are compiled in Table II. These

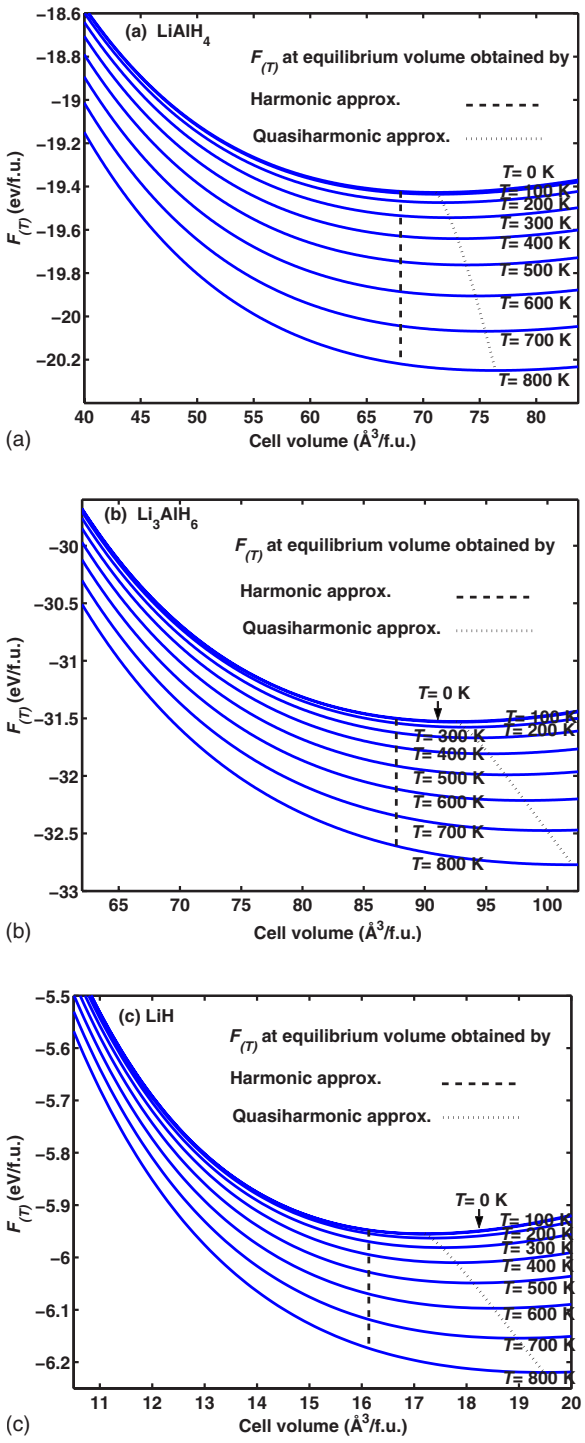

FIG. 2. (Color online) Calculated Helmholtz free energy $F_{(T)}$ as a function of cell volume for (a) $LiAlH_4$, (b) Li_3AlH_6, and (c) LiH in the temperature range from 0 to 800 K. The dashed lines indicate the position of the equilibrium cell volume. The blue solid curves represent QHA results.

values of expansivities of the lithium alanates are similar to those of the sodium alanates.[45]

Once the equilibrium volume is known, the thermodynamic functions can be obtained as described above. The calculated and measured thermodynamic functions as a function of temperature for $LiAlH_4$ are presented in Fig. 3. It is seen that the calculated thermodynamic functions are in good agreement with the corresponding experimental data over a large temperature range. It is noted that the thermodynamic functions obtained from the HA and the QHA are nearly identical at lower temperatures (up to the melting point of 453 K), whereas at higher temperatures the QHA produces results larger than those obtained from the HA. It should be mentioned that the validity of the (Q)HA approximation may become questionable above the melting point. We note that several recent studies on the liquid phases of $LiBH_4$ (Refs. 13 and 34) and $Li_4BN_4H_{10}$ (Ref. 35) have modeled the dehydrogenation reactions as solid-state reactions using the HA due to the high computational costs associated with the calculations for the liquid phases. This may be justified to some extent as the liquid phases have more positive enthalpy values than the corresponding solids. Consequently, the calculated solid-state enthalpy can be regarded as an upper bound on the enthalpy for the hydrogen desorption from the liquids.[35] In the present work, our main focus is on the stability and reaction reversibility of the solid-state lithium alanates below the melting point, where both HA and QHA produce results in good agreement with the experimental data.

The calculated thermodynamic functions as a function of temperature for Li_3AlH_6 and LiH are shown in Figs. 4 and 5, respectively. Again, the results calculated by the QHA are larger than those by the HA, particularly at high temperatures. Experimental data for Li_3AlH_6 are not yet available at present. The calculated data provide a systematic description for its thermodynamic properties over a large range of temperature; these data can be used to further calculate other physical properties of interest (see below) or as input in other theoretical (e.g., empirical) studies. For LiH, the calculated thermodynamic functions are in good agreement with the experimental data. Figure 5(b) shows that the QHA is in a slightly better agreement with the experiment than the HA. However, for Figs. 5(a) and 5(c), the reverse is true, i.e., the HA is in a better agreement with the experiment than the QHA (in particular, $T>450$ K). Figure 5(c) shows that the free-energy changes obtained from these two methods are close to each other at $T<450$ K, and the QHA overestimates the experimental data at $T>450$ K. According to these results, neither method has a clear advantage when $T>450$ K.

The above results show that our calculated thermodynamic functions of the lithium alanates are in good agreement with available experimental data, especially at lower temperatures (below 450 K). Deviations from the experimental data appear at higher temperatures. In general, the QHA tends to overestimate and the HA tends to underestimate these thermodynamic functions. In all the cases considered here, the HA and QHA results seem to provide the lower and upper bounds (in magnitude) for the thermodynamic functions. For the purpose of on-board hydrogen storage, the required temperature should be lower than 450 K, and thus both the HA and the QHA can provide reliable data for the thermodynamic calculations.

TABLE II. Temperature-dependent equilibrium volume and thermal expansivity $\left(\alpha=\frac{1}{V}\frac{\partial V}{\partial T}\right)$ for $LiAlH_4$, Li_3AlH_6, and LiH in the temperature range from 0 to 800 K.

Temperature (K)	0	100	200	300	400	500	600	700	800
Volume for $LiAlH_4$ (Å^3)	71.1	71.3	71.7	72.3	73.0	73.8	74.6	75.5	76.4
α for $LiAlH_4$ (10^{-4}) (K)	0	0.44	0.75	0.94	1.06	1.12	1.17	1.23	1.35
Volume for Li_3AlH_6 (Å^3)	92.6	92.7	93.2	94.1	95.2	96.6	98.1	99.9	102.0
α for Li_3AlH_6 (10^{-4}) (K)	0	0.38	0.78	1.09	1.34	1.57	1.82	2.11	0.248
Volume for LiH (Å^3)	17.2	17.2	17.3	17.5	17.8	18.2	18.5	18.9	19.5
α for LiH (10^{-4}) (K)	0	0.41	0.92	1.35	1.73	2.08	2.42	2.79	3.22

B. Decomposition reactions for $LiAlH_4$ and Li_3AlH_6 at atmospheric pressure

In the preceding section, we presented the calculated thermodynamic functions of the lithium alanates that are in good agreement with experimental values. In this section, we use these functions to study the chemical reactions described in Eqs. (1) and (2).

Figure 6 shows the calculated enthalpy changes and Gibbs free-energy changes as a function of temperature at atmospheric pressure. The results are calculated by both the QHA and the HA. In the preceding section, the calculations show that the thermodynamic functions obtained from the QHA are always larger than those obtained from the HA, in particular, at high temperatures, e.g., for Li_3AlH_6 at $T=800$ K, the free-energy difference between the QHA and the HA is 0.2 eV/f.u. (see Fig. 4). As a result, one may expect that there must be some differences in the reaction energies obtained from these two methods. However, Fig. 6 shows that

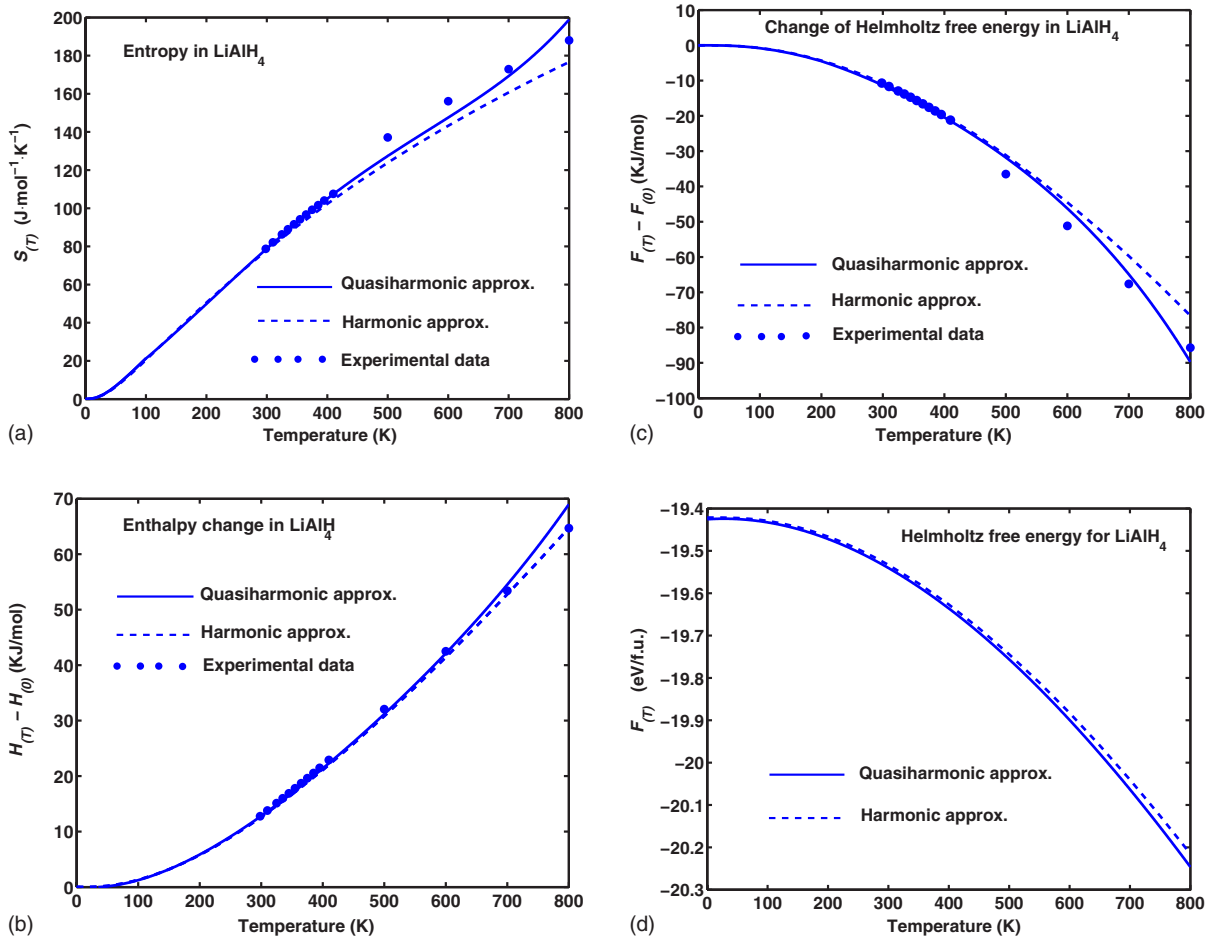

FIG. 3. (Color online) Calculated (lines) and measured (dots) thermodynamic functions of $LiAlH_4$ as a function of temperature. (a), (b), (c), and (d) represent entropy ($S_{(T)}$), enthalpy change ($H_{(T)}-H_{(0)}$), change of Helmholtz free energy ($F_{(T)}-F_{(0)}$), and Helmholtz free energy ($F_{(T)}$), respectively. Solid and dashed lines represent calculated results from quasiharmonic and harmonic approximations, respectively. Measured data are from tabulated thermochemical data (Ref. 32).

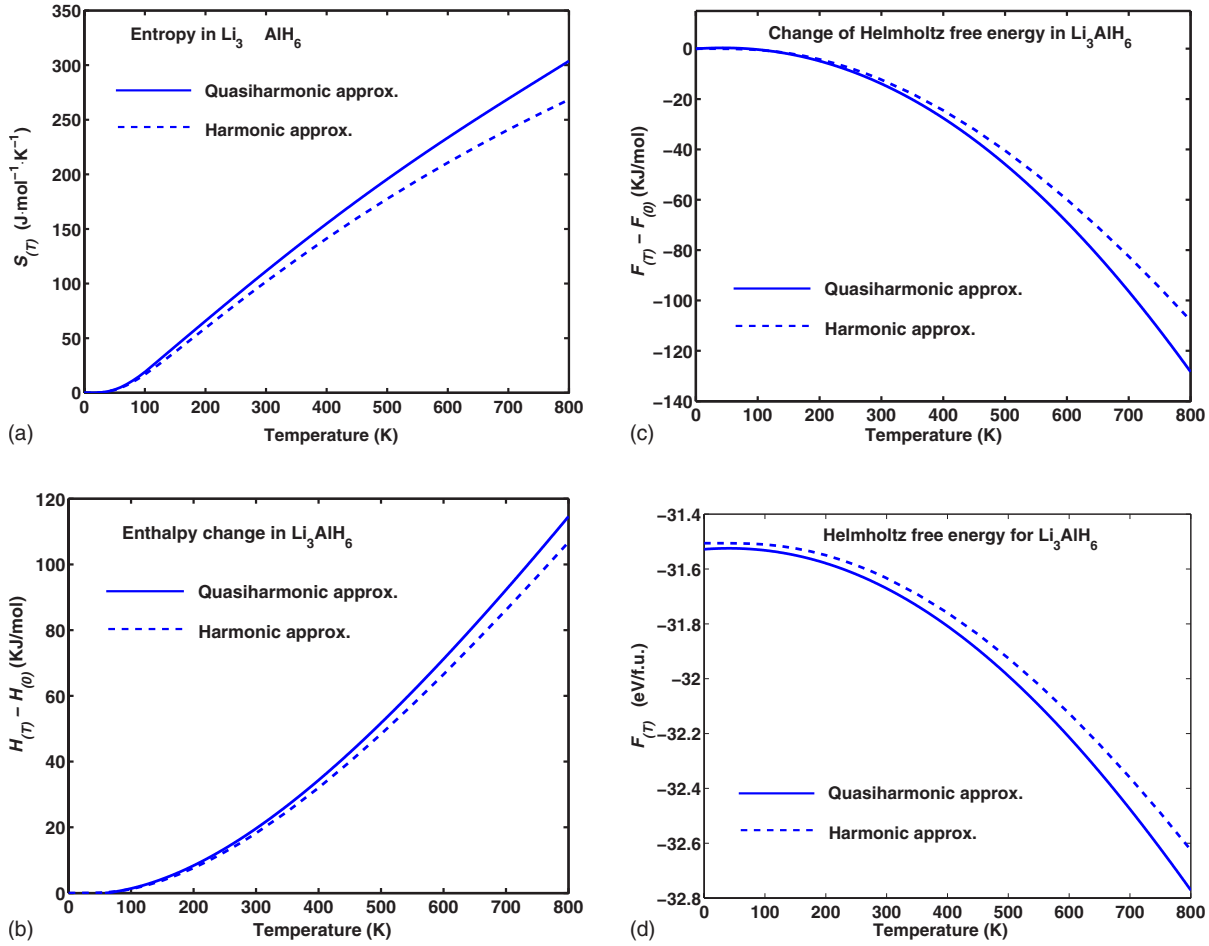

FIG. 4. (Color online) Calculated thermodynamic functions of Li_3AlH_6 as a function of temperature. (a), (b), (c), and (d) represent entropy ($S_{(T)}$), enthalpy change ($H_{(T)}-H_{(0)}$), change of Helmholtz free energy ($F_{(T)}-F_{(0)}$), and Helmholtz free energy ($F_{(T)}$), respectively. Solid and dashed lines represent calculated results from quasiharmonic and harmonic approximations, respectively. No experimental data are available for Li_3AlH_6.

the actual difference is quite small. The reason for this outcome is that the thermodynamic functions calculated by the QHA have the same trend for both the reactant and product, i.e., both are larger than those calculated by the HA. The reaction enthalpy (or reaction free energy) is calculated by the energy *differences* between the reactant and product and thus the energy differences are largely canceled out. It shows that the HA is as good as the QHA in calculating (with much lower computing costs) the reaction enthalpy and reaction free energy for the hydrides at atmospheric pressure. This is also because the pV term has little contribution to the enthalpy compared to the energy term. However, at elevated pressures, this contribution becomes important. Since the HA does not consider the volume change in response to temperature variation (see Fig. 2), the QHA must be employed at elevated pressures.

Figure 6(b) shows that the Gibbs free-energy change for Eq. (1) is negative at all temperatures, indicating that the decomposition of $LiAlH_4$ takes place spontaneously. This is in accordance with existing experimental observation[16–18] and theoretical predication.[12] For Eq. (2), the positive enthalpy change shown in Fig. 6(a) indicates that the reaction is endothermic; the negative Gibbs free-energy change at $T > 180$ K [Fig. 6(b)] indicates that the decomposition of Li_3AlH_6 takes place spontaneously at $T > 180$ K. This is also in accordance with another theoretical predication.[12] Based on these calculations at 1 atm, we conclude that the reaction for Eq. (1) is irreversible, and the reaction for Eq. (2) also is irreversible when the temperature exceeds ~180 K.

So far, we have focused on the calculations at atmospheric pressure. In the next section, we will examine the reactions of Eqs. (1) and (2) at elevated pressures.

C. Phase diagram for $LiAlH_6$ Li_3AlH_6, and LiH

To study the phase diagram for the reactions in Eqs. (1) and (2), we need to examine the Gibbs free energy of H_2 gas at elevated pressures. The free energy at elevated pressures is calculated by

$$G_{(p,T)}(\mathrm{H_2}) = G_{(p_0=1\ \mathrm{atm},T)}(\mathrm{H_2}) + k_B T \ln\left(\frac{\gamma p}{p_0}\right), \qquad (9)$$

where p_0 and p denote atmospheric and elevated pressures, respectively, and γ is the hydrogen fugacity coefficient. The fugacity measures the deviation of a real gas from the ideal behavior ($\gamma=1$ describes an ideal gas). This property is im-

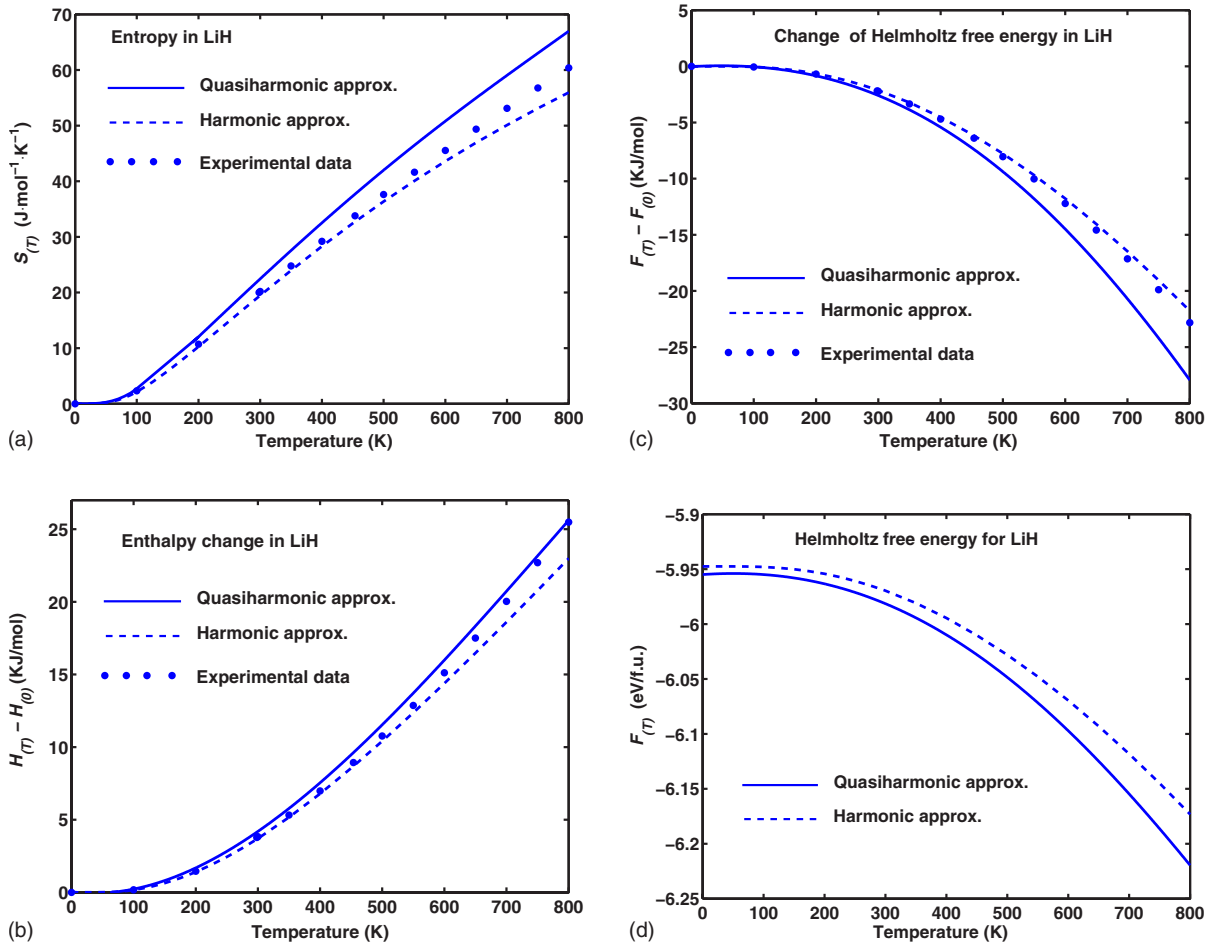

FIG. 5. (Color online) Calculated and measured thermodynamic functions of LiH as a function of temperature. (a), (b), (c), and (d) represent entropy ($S_{(T)}$), enthalpy change ($H_{(T)}-H_{(0)}$), change of Helmholtz free energy ($F_{(T)}-F_{(0)}$), and Helmholtz free energy ($F_{(T)}$), respectively. Solid and dashed lines represent calculated results from quasiharmonic and harmonic approximations, respectively. Measured data (in dots) are from tabulated thermochemical data (Ref. 32).

portant at relatively high pressures (e.g., see Refs. 46 and 47). To know how much γ contributes to the free energy, the logarithmic fugacity coefficient $\ln \gamma$ as a function of hydrogen pressure is plotted in Fig. 7. The dots are the data at $T=298$ K from Ref. 48, in which the data below 3000 atm were directly calculated from the experimental values,[49] and the data above 3000 atm were extrapolated from the virial expansion. The solid lines at different temperatures are from Ref. 50, in which the fugacity coefficients were calculated from the Beattie-Bridgeman equation of state.[51] The figure shows that the contribution from the fugacity cannot be neglected at high pressure, e.g., at $T=298$ K and $p=1$ GPa, $\ln \gamma$ is equal to 6.0, which means that the contribution to the free energy is 0.154 eV per H_2 molecule (i.e., $6k_BT$). It is noted that the contribution at low pressures is negligible, e.g., at $T=298$ K and $p=100$ atm, $\ln \gamma$ is equal to 0.07, which is equivalent to a contribution of only 0.002 eV per H_2 to the free energy. Below, we will choose the data from Ref. 50 for our calculations because these data are much more complete than those from Ref. 48.

Once the Gibbs free energies of these hydrides as a function of pressure and temperature are known, the phase diagrams can be determined from the following procedure: first, at a given temperature, the Gibbs free energies for the hydrides as a function of pressure are plotted; then, a coexistence point between the lines may be found; finally, by varying the temperature, the (pT) phase diagram are constructed by collecting all the coexistence points.

Figure 8 shows the Gibbs free energy as a function of pressure for the reactant and product in Eq. (1) at $T=273$ K. The results show that the product is always more stable than the reactant, and thus there is no coexistence point between these two lines. Varying the temperature, we found that the situation is the same, i.e., the product is always more stable than the reactant. Frankcombe and Kroes[12] recently predicted that $LiAlD_4$ is slightly more stable than $LiAlH_4$ at atmospheric pressure. It is interesting to see whether there is a coexistence point between the deuterated reactant ($LiAlD_4$) and the deuterated product $(\frac{1}{3}Li_3AlD_6+\frac{2}{3}Al+D_2)$ at elevated pressures. The calculated Gibbs free energies shown in Fig. 8 indicate that there is a down shift in their free energies, but there is still no coexistence point between these two lines. The situation remains the same over a large temperature range that we examined. Based on these results, we conclude that $LiAlH_4$ and $LiAlD_4$ always tend to decompose under all temperature and pressure conditions,

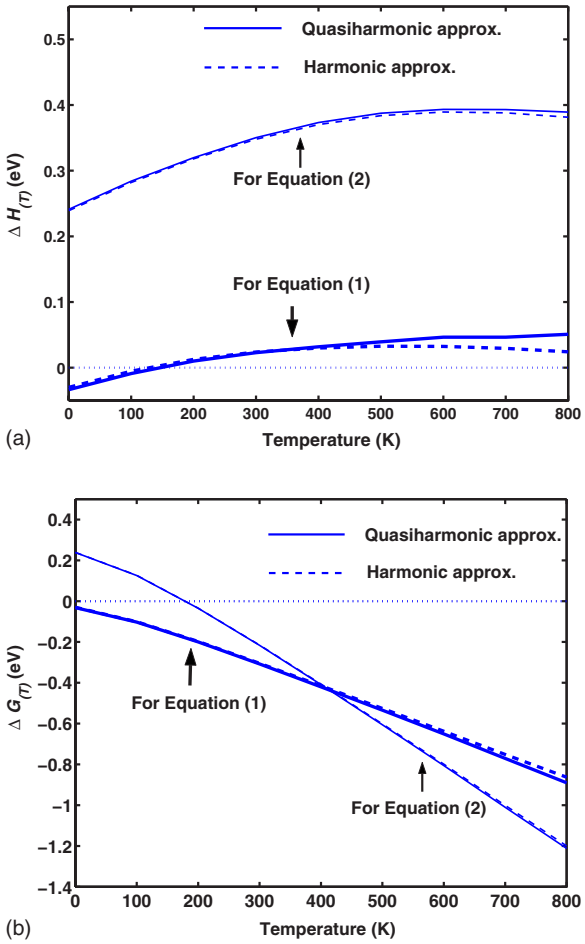

FIG. 6. (Color online) Calculated (A) enthalpy changes and (B) Gibbs free-energy changes as a function of temperature at atmospheric pressure for Eqs. (1) and (2). Thick and thin lines represent the results for Eqs. (1) and (2), respectively. Solid and dashed lines represent the results calculated using the quasiharmonic and harmonic approximations, respectively.

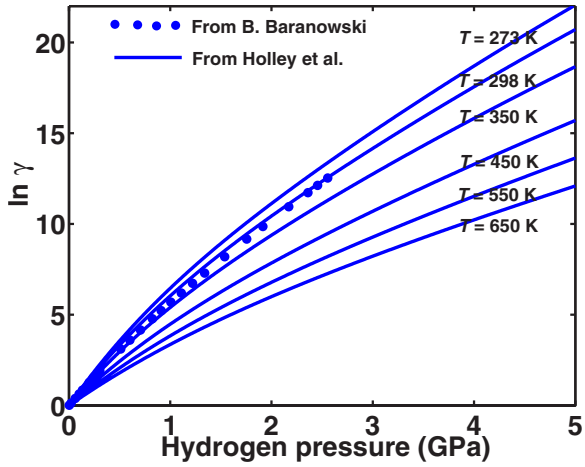

FIG. 7. (Color online) Logarithmic hydrogen fugacity coefficient ln γ as a function of hydrogen pressure. The dots are the data at $T=298$ K (Ref. 48). The solid lines are the data from (Ref. 50).

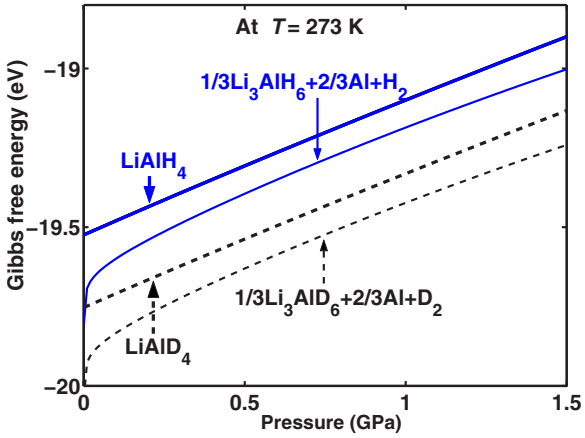

FIG. 8. (Color online) Gibbs free energy as a function of pressure for the reactant and product in Eq. (1) at 273 K. Thick and thin solid lines represent the energies for $LiAlH_4$ and $\left(\frac{1}{3}Li_3AlH_6+\frac{2}{3}Al+H_2\right)$, respectively. Thick and thin dashed lines represent the energies for $LiAlD_4$ and $\left(\frac{1}{3}Li_3AlD_6+\frac{2}{3}Al+D_2\right)$, respectively.

indicating that the reaction of Eq. (1) is irreversible. It is noted that the fugacity of the D_2 gas is not available from experiment; instead, the fugacity of H_2 was used in our calculations. To estimate its effect on the calculated results, we note that, in principle, a gas with a larger mass will deviate more from the ideal behavior than that with a small mass, and thus the fugacity for the N_2 gas should be larger than that of the D_2 gas, which in turn should be larger than that for the H_2 gas. The fugacity coefficient ln γ for the N_2 gas is known to be about twice as large as that for H_2 at $T=273$ K and $p=1$ GPa.[50] It is equivalent to an extra contribution of 0.047 eV per molecule to the free energy. The extra contribution from D_2 should be smaller than this value. Such a small change in free energy will not affect the conclusions drawn in the present work.

Using the same procedure, we now analyze the stability of Li_3AlH_6 in Eq. (2). Unlike the situation for $LiAlH_4$, here there is always a cross (coexistence) point between the Gibbs free-energy curves of the reactant and the product. This means that the relative stability of the reactant and the product can be switched, thus allowing the release and recharge of hydrogen under appropriate temperature and pressure conditions, which is a key requirement for any practical hydrogen-storage medium. Figure 9 shows the Gibbs free energy as a function of pressure for the reactant and the product at $T=273$ K. At this temperature, the coexistence pressure is 100 atm. We carried out calculations for the coexistence pressure points at various temperatures. The results are compiled in Table III. Based on these results, the (p,T) phase diagram for the reactant (Li_3AlH_6) and the product $\left(3LiH+Al+\frac{3}{2}H_2\right)$ is constructed, as shown in Fig. 10. The filled shadow area indicates the phase space where Li_3AlH_6 can be stabilized, and the area outside of the shadow is where Li_3AlH_6 decomposes into the product $\left(3LiH+Al+\frac{3}{2}H_2\right)$. It is noted that the reaction of $LiH \rightarrow Li+\frac{1}{2}H_2$ will not affect this phase diagram since this reaction only takes place at much higher temperatures (823 K).[52] The boundary between these two areas can be fitted to the van't Hoff equation,[53]

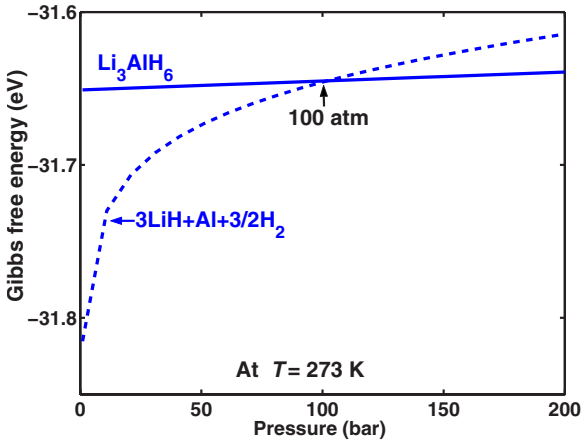

FIG. 9. (Color online) Gibbs free energy as a function of pressure for the reactant and product in Eq. (2) at $T=273$ K. The solid and dashed lines represent the energies for Li_3AlH_6 and $\left(3LiH+Al+\frac{3}{2}H_2\right)$, respectively.

$$\ln\frac{p}{p_0} = -\frac{\Delta H_R}{RT} + \frac{\Delta S_R}{R}, \tag{10}$$

where p_0 is the atmospheric pressure ($p_0=1$), p is the equilibrium hydrogen pressure, R is the gas constant, ΔH_R is the overall reaction enthalpy, and ΔS_R is the entropy change. Usually, the overall reaction enthalpy ΔH_R is considered to be closely related to the enthalpy of formation ΔH (e.g., see Ref. 33). However, the situation is different in the present case, since the decomposition of Li_3AlH_6 takes place spontaneously at ambient conditions and thus the ΔH was obtained without considering the phase equilibrium [Fig. 6(a) shows the plot of the enthalpy change (ΔH) only at one pressure (i.e., at atmospheric pressure); the equilibrium pressure for the reaction is not considered there]. However, ΔH_R is determined from the equilibrium hydrogen pressure and temperature. Therefore, the meaning of ΔH_R is different from that of ΔH, and the latter cannot be used to construct the phase diagram.

A fitting to our calculated results leads to

$$\ln p = -\frac{0.22}{RT} + 13.89, \tag{11}$$

which gives $\Delta H_R=0.22$ eV. The value of ΔH_R is very important since it determines the slope of the line and thus controls the equilibrium hydrogen pressure at a given temperature. For the purpose of hydrogen storage, the optimum value for

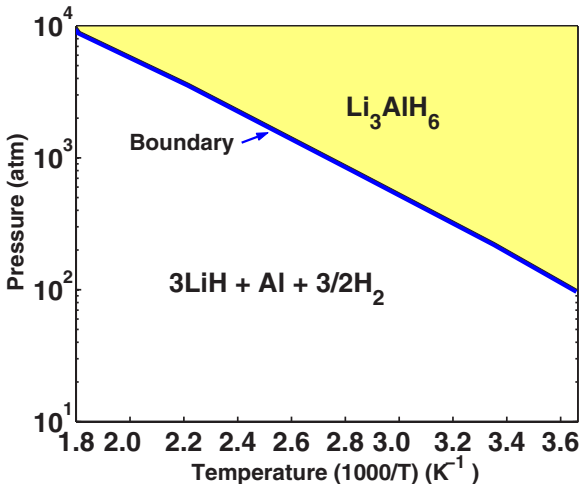

FIG. 10. (Color online) The (p,T) phase diagram for the reactant (Li_3AlH_6) and the product $\left(3LiH+Al+\frac{3}{2}H_2\right)$ in Eq. (2).

ΔH_R is 0.41 eV per H_2, which makes the hydrogen storage reversible at around $p=1$ atm and $T=300$ K.[54] The value of 0.22 eV for Li_3AlH_6 is smaller than this ideal value, which means that an applied pressure is needed to make this material reversible at a given temperature. From Fig. 10, it can be seen that the equilibrium pressure is 227 atm at $T=298$ K. Therefore, to use this material as a hydrogen-storage medium, the choice of appropriate catalysts will be necessary to decrease the required equilibrium pressure. It is noted that there are also coexistence points between the Gibbs free energies of the deuterated reactant (Li_3AlD_6) and the deuterated product $\left(3LiD+Al+\frac{3}{2}D_2\right)$. Since the fugacity of the D_2 gas is not available from experiment, the phase diagram for the Li_3AlD_6 is not presented in this paper. By using the fugacity of H_2, the pressure for the deuterated phase diagram at a given temperature was found to be higher than that for the preceding result. This seems to be incorrect.

Finally, we comment on two recent experiments related to Eq. (2). In the experiment of Chen *et al.*,[15] this reaction was reported to be reversible, and the measured value for ΔH_R is 0.43 eV per H_2. This value is nearly identical to the optimum value of 0.41 eV per H_2 for hydrogen storage at ambient condition. However, this result has yet to be reproduced by other groups. Very recently, using similar catalysts, Brinks *et al.*[16] reported that the equilibrium pressure for this reaction is at least 85 bars at 353 K. It indicates that this reaction may be reversible but only at relatively high pressures. Our theoretical result is consistent with this latest experiment. A key open question is the role of the catalyst in these two experi-

TABLE III. Coexistence pressure points between the reactant (Li_3AlH_6) and product $\left(3LiH+Al+\frac{3}{2}H_2\right)$ in Eq. (2) at various temperatures.

	Temperature (K)				
	273	298	350	450	550
Pressure at coexistence points (atm)	100	227	820	3676	9056

ments, particularly the seemingly different effect of the catalysts on the equilibrium pressure. This issue deserves further attention by careful modeling and much more extensive (and expensive) computational studies.

IV. CONCLUSIONS

We have presented a systematic computational study on the thermodynamic properties and phase stability of lithium alanates $LiAlH_4$, Li_3AlH_6, and LiH using density-functional theory (at GGA level) and quasiharmonic phonon calculations. The calculated thermodynamic functions are in good agreement with available experimental data. Based on these thermodynamic functions, the relative phase stabilities of these alanates are examined. The decomposition of $LiAlH_4$ is found to be irreversible under all temperature and pressure conditions considered, indicating that a direct synthesis of $LiAlH_4$ from the solid reaction of $\left(\frac{1}{3}Li_3AlH_6+\frac{2}{3}Al+H_2\right)$ is not possible. Meanwhile, the calculations indicate that Li_3AlH_6 can be used as a rechargeable hydrogen-storage medium under applied pressures. We constructed the (p,T) phase diagram for Li_3AlH_6. By fitting the obtained phase boundary to the van't Hoff equation, the overall reaction enthalpy of 0.22 eV is obtained. Our calculated results are consistent with the latest experiment by Brinks *et al.*[16]

ACKNOWLEDGMENTS

Work at UNLV was supported by the U.S. Department of Energy Grants No. DE-FG36-05GO085028 and No. DE-FC52-06NA26274. X.K. was also supported by National Natural Science Foundation of China with Grants No. 10504007 and No. 10635040, and Shanghai Supercomputer Center.

*Electronic address: ke@physics.unlv.edu, xzke@yahoo.com
†Electronic address: chen@physics.unlv.edu

[1] J. H. Hirschenhofer, D. B. Stauffer, and R. R. Engleman, *Fuel Cells: A Handbook* (U.S. Department of Energy, Morgantown, West Virginia, 1994).
[2] B. Bogdanović and M. Siward, J. Alloys Compd. **253**, 1 (1997).
[3] B. Bogdanović, R. A. Brand, A. Marjanović, M. Schwickardi, and J. Tölle, J. Alloys Compd. **302**, 36 (2000).
[4] K. J. Gross, S. Guthrie, S. Takara, and G. Thomas, J. Alloys Compd. **297**, 270 (2000).
[5] C. M. Jensen and K. J. Gross, Appl. Phys. A: Mater. Sci. Process. **72**, 213 (2001).
[6] B. Yebka and G. A. Nari, Mater. Res. Soc. Symp. Proc. **801**, 133 (2004).
[7] P. Vajeeston, P. Ravindran, R. Vidya, H. Fjellvåg, and A. Kjekshus, Appl. Phys. Lett. **82**, 2257 (2003).
[8] A. Aguayo and D. J. Singh, Phys. Rev. B **69**, 155103 (2004).
[9] S. M. Opalka and D. L. Anton, J. Alloys Compd. **356**, 486 (2003).
[10] M. E. Arroyo y de Dompablo and G. Ceder, J. Alloys Compd. **364**, 6 (2004).
[11] O. M. Løvvik, S. M. Opalka, H. W. Brinks, and B. C. Hauback, Phys. Rev. B **69**, 134117 (2004).
[12] T. J. Frankcombe and G.-J. Kroes, Chem. Phys. Lett. **423**, 102 (2006).
[13] T. J. Frankcombe and G.-J. Kroes, Phys. Rev. B **73**, 174302 (2006).
[14] J.-W. Jang, J. H. Shim, Y. W. Cho, and B. J. Lee, J. Alloys Compd. **420**, 286 (2006).
[15] J. Chen, N. Kuriyama, Q. Xu, H. T. Takeshita, and T. Sakai, J. Phys. Chem. B **105**, 11214 (2001).
[16] H. W. Brinks, A. Fossdal, J. E. Fonneløp, and B. C. Hauback, J. Alloys Compd. **397**, 291 (2005).
[17] T. N. Dymova, D. P. Aleksandrov, V. N. Konoplev, T. A. Silina, and A. S. Sizareva, Russ. J. Coord. Chem. **20**, 263 (1994).
[18] N. N. Mal'tseva and A. I. Golovanova, Russ. J. Appl. Chem. **73**, 747 (2000).
[19] W. Kohn and L. J. Sham, Phys. Rev. **140**, A1133 (1965).
[20] P. Hohenberg and W. Kohn, Phys. Rev. **136**, B864 (1964).
[21] J. P. Perdew, J. A. Chevary, S. H. Vosko, K. A. Jackson, M. R. Pederson, D. J. Singh, and C. Fiolhais, Phys. Rev. B **46**, 6671 (1992).
[22] G. Kresse and J. Furthmüller, Comput. Mater. Sci. **6**, 15 (1996).
[23] G. Kresse and J. Furthmüller, Phys. Rev. B **54**, 11169 (1996).
[24] P. E. Blöchl, Phys. Rev. B **50**, 17953 (1994).
[25] G. Kresse and D. Joubert, Phys. Rev. B **59**, 1758 (1999).
[26] H. J. Monkhorst and J. D. Pack, Phys. Rev. B **13**, 5188 (1976).
[27] K. Parlinski, Z. Q. Li, and Y. Kawazoe, Phys. Rev. Lett. **78**, 4063 (1997).
[28] K. Parlinski, Software PHONON, Institute of Nuclear Physics, Crakow, 2005.
[29] A. A. Maradudin, E. W. Montroll, G. H. Weiss, and I. P. Ipatova, *Theory of Lattice Dynamics in The Harmonic Approximation*, Solid State Physics Supplement Vol. 3 (Academic, New York, 1971).
[30] G. J. Ackland, J. Phys.: Condens. Matter **14**, 2975 (2002).
[31] M. Born and K. Huang, *Dynamical Theory of Crystal Lattices* (Oxford University Press, New York, 1954).
[32] D. R. Stull and H. Prophet, *JANAF Thermochemical Tables*, 2nd ed. (U.S. National Bureau of Standards, Washington, DC, 1971).
[33] J. F. Herbst and L. G. Hector Jr., Phys. Rev. B **72**, 125120 (2005).
[34] K. Miwa, N. Ohba, S. Towata, Y. Nakamori, and S. Orimo, Phys. Rev. B **69**, 245120 (2004).
[35] D. J. Siegel, C. Wolverton, and V. Ozoliņš, Phys. Rev. B **75**, 014101 (2007).
[36] G. D. Barrera, D. Colognesi, P. C. H. Mitchell, and A. J. Ramirez-Cuesta, Chem. Phys. **317**, 119 (2005).
[37] G. Roma, C. M. Bertoni, and S. Baroni, Solid State Commun. **98**, 203 (1996).
[38] J. L. Anderson, J. Nasise, K. Philipson, and F. E. Pretzel, J. Phys. Chem. Solids **31**, 613 (1970).
[39] P. Vajeeston, P. Ravindran, R. Vidya, H. Fjellvåg, and A. Kjekshus, Phys. Rev. B **68**, 212101 (2003).
[40] B. C. Hauback, H. W. Brinks, and H. Fjellvåg, J. Alloys Compd. **346**, 184 (2002).
[41] P. Vajeeston, P. Ravindran, A. Kjekshus, and H. Fjellvåg, Phys.

Rev. B **69**, 020104(R) (2004).
[42] H. W. Brinks and B. C. Hauback, J. Alloys Compd. **354**, 143 (2003).
[43] S. Baroni, S. de Gironcoli, and A. D. Corso, Rev. Mod. Phys. **73**, 515 (2001).
[44] F. Birch, Phys. Rev. **71**, 809 (1947).
[45] X. Ke and I. Tanaka, Phys. Rev. B **71**, 024117 (2005).
[46] J. Graetz, S. Chaudhuri, Y. Lee, T. Vogt, J. T. Muckerman, and J. J. Reilly, Phys. Rev. B **74**, 214114 (2006).
[47] P. Kroll, T. Schröter, and M. Peters, Angew. Chem., Int. Ed. **44**, 4249 (2005).
[48] B. Baranowski, Ber. Bunsenges. Phys. Chem. **76**, 714 (1972).
[49] W. de Graaff, Ph.D. thesis, University of Amsterdam, Amsterdam, 1960.
[50] C. E. Holley Jr., W. J. Worlton, and R. K. Zeigler, Los Alamos Science Laboratory, Report No. LA-2271, 1958 (unpublished).
[51] J. A. Beattie and O. C. Bridgeman, J. Am. Chem. Soc. **50**, 3133 (1928).
[52] P. Chen, Z. Xiong, J. Luo, J. Lin, and K. L. Tan, J. Phys. Chem. B **107**, 10967 (2003).
[53] K. H. J. Buschow, in *Handbook on the Physics and Chemistry of Rare Earths*, edited by K. A. Gschneidner, Jr. and L. Eyring (North-Holland, Amsterdam, 1984), Vol. 6.
[54] L. Schlapbach and A. Züttle, Nature (London) **414**, 353 (2001).